Accurate Extraction of Anisotropic Spin-Orbit Torques from Harmonic Measurements

D.M.J. van Elst,[1, a)] M.R.A. Peters,[1, a)] F. Büttner,[2, 3, b)] A. Wittmann,[2] E.A. Tremsina,[2, 4] C. O. Avci,[5] R. Lavrijsen,[1] H.J.M. Swagten,[1] and G.S.D. Beach[2]

[1)] *Department of Applied Physics, Eindhoven University of Technology, P.O. Box 513, 5600MB Eindhoven, The Netherlands*

[2)] *Department of Materials Science and Engineering, Massachusetts Institute of Technology, Cambridge, MA 02142, USA*

[3)] *Helmholtz-Zentrum für Materialien und Energie GmbH, 14109 Berlin, Germany*

[4)] *Department of Electrical Engineering and Computer Science, Massachusetts Institute of Technology, Cambridge, MA 02142, USA*

[5)] *Department of Materials, ETH Zürich, CH-8093 Zürich, Switzerland*

(Dated: 30 April 2021)

One of the most powerful ways to manipulate spins in nanometer-scale devices is by converting a charge current to a spin current via spin-orbit coupling. The resulting spin-orbit torques (SOTs) have been investigated and utilized extensively in the past decade. Quantitatively, however, SOTs may exhibit a non-trivial angular dependence which is not well explored. Here, we develop a nested iterative analysis to determine the magnitude of SOTs from harmonic Hall measurements. This updated method largely improves the fit quality in the full magnetic field range and accurately retrieves even higher order, anisotropic spin-orbit torque coefficients. The numerical implementation of our algorithm is fast, robust, and designed for easy integration into existing analysis schemes. We verify our code using simulated data with and without anisotropic SOTs. Accurately quantifying higher order SOT terms can be especially useful for modeling non-uniform magnetic textures such as domain walls and skyrmions and current-induced magnetization switching characteristics.

In a thin-film magnetic heterostructure with broken inversion symmetry, a longitudinal electrical current can be converted to a spin current via spin-orbit coupling effects near material interfaces. The spin currents can subsequently exert a torque on the local magnetization of the magnetic thin film. These torques are known as spin-orbit torques (SOTs) and offer great potential for spintronic devices.[1,2] For example, it has already been shown that SOT can be used for magnetic switching with high efficiency[3,4], for nucleating and annihilating magnetic skyrmions[5,6], and for driving domain walls[7,8] and skyrmions[9–12] into motion.

Spin-orbit torques are often approximated by two isotropic torque terms, the isotropic antidamping-like torque and the isotropic field-like torque. These torques can be quantified by single, scalar, material-dependent proportionality constants: the effective spin Hall angle and the field-like spin-orbit torque efficiency, respectively. However, recent experiments, in particular on heavy metal/ferromagnetic metal/oxide (HM/FM/Ox) heterostructures, have shown that the magnitude of SOTs also depends on the magnetization direction.[13–18] This anisotropic behavior is attributed to spin-orbit coupling driven effects at the HM/FM interface.[2,19–21] Since domain walls and skyrmions inherently include spins of every possible orientation, even small anisotropies of the SOTs may considerably alter the resulting current-driven dynamics of such textures. The relevance of taking anisotropy into account when evaluating dynamics in spin textures has recently been shown.[22] A detailed understanding and accurate modeling of such anisotropic torques is hence highly desirable.

Harmonic Hall measurements provide a sensitive tool to quantify SOTs, including their angular dependence.[13,18,23] The analysis of such data is well-established for the case of isotropic SOTs.[13,14,23,24] By contrast, for the measurement of anisotropic higher order terms, though explored in the past[15,17–19,25], a self-consistent analysis scheme is not available. Here, we analyze simulated harmonic signals and evaluate how precisely the simulation model parameters can be extracted from the data. We find that the existing iterative approach to analyze harmonic measurements performs well for the leading order coefficient but fails to reproduce large anisotropic higher order terms. We develop a nested iterative procedure and show that with this approach, terms up to at least the fourth order are accurately extracted in a self-consistent manner.

We consider an electrically contacted strip of a thin-film, perpendicular magnetic material, as illustrated in Fig. 1a. The current direction is defined as the x-direction and the out-of-plane magnetic easy axis is along the z-direction. θ and ϕ denote the polar and azimuthal angles and added indices "eq" and "b" indicate the equilibrium direction without current and the direction of the external magnetic field, respectively. We consider the typical case of a material with negligible in-plane anisotropy, i.e. $\phi_{eq} = \phi_b$.[13] In this configuration, the effective fields corresponding to the field-like (FL) and antidamping-like (AD) spin-orbit torques due to a cur-

———————

[a)] These authors contributed equally to this work

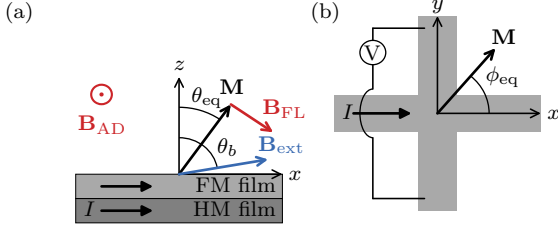[b)] Electronic mail: felix.buettner@helmholtz-berlin.de

FIG. 1: Geometry and coordinate system. (a) Side view of the Hall bar structure. $\mathbf{M}$ is the magnetization, $\mathbf{B}_{\text{ext}}$ the external applied field. θ_{eq} and θ_b are the azimuthal angles of the magnetization and external applied field from the z-axis, respectively. $\mathbf{B}_{\text{AD}}$, $\mathbf{B}_{\text{FL}}$ are the effective SOT fields. (b) Top view of the Hall bar structure indicating the in-plane angle ϕ_{eq} of the magnetization, as well as the measurement direction of the transverse voltage.

rent I can be written as[13]

$$\mathbf{B}_{\text{FL}} = c\sin(\phi_{\text{eq}})[B_0^{\text{FL}} + s^2 B_2^{\text{FL}} + s^4 B_4^{\text{FL}} + \ldots]\hat{\mathbf{e}}_\theta \\ + \cos(\phi_{\text{eq}})B_0^{\text{FL}}\hat{\mathbf{e}}_\phi \qquad (1)$$

and

$$\mathbf{B}_{\text{AD}} = -\cos(\phi_{\text{eq}})[B_0^{\text{AD}} + s^2 B_2^{\text{AD}} + s^4 B_4^{\text{AD}} + \ldots]\hat{\mathbf{e}}_\theta \\ + c\sin(\phi_{\text{eq}})B_0^{\text{AD}}\hat{\mathbf{e}}_\phi, \qquad (2)$$

where $c = \cos(\theta_{\text{eq}})$ and $s = \sin(\theta_{\text{eq}})$ throughout this text. The lowest order field coefficients B_0^{FL} and B_0^{AD} in Eqs. (1) and (2) represent the isotropic SOT, which, on their own, can be written as $\mathbf{B}_0^{\text{FL}} \propto \hat{\mathbf{y}} \times \mathbf{M}$ and $\mathbf{B}_0^{\text{AD}} \propto \hat{\mathbf{y}}$. The higher order coefficients $B_{2,4}^{\text{FL}}$ and $B_{2,4}^{\text{AD}}$ introduce a non-trivial dependence of the polar SOT component on the magnetization direction. Note that higher order terms in the azimuthal component are also allowed in principle, but were never observed experimentally (potentially due to the lower sensitivity of harmonic measurements to changes in ϕ) and therefore neglected here[2,13]; if needed, it is straightforward to extend the analysis presented below to include such terms.

To determine the SOT coefficients by harmonic Hall measurement, we consider a Hall bar geometry as depicted in Fig. 1b with an AC current $I(t) = I_0\cos(2\pi f t)$. The anomalous (AHE) and planar (PHE) Hall effect lead to a transverse (Hall) voltage V_{H} in this geometry. To account for the dynamic change of the resistance due to the spin-torque-induced rotation of the magnetization, the Hall voltage can be expanded in terms of harmonics of f as $V_{\text{H}}(t) = \sum_n V^{nf}\cos(2\pi n f t)$. The $V^{nf} = I_0 R^{nf}$ harmonics can be measured individually using, e.g., a lock-in amplifier. The first and second order resistance coefficients can be analytically related to the magnetic properties of the material via[13]

$$R_{\text{H}}^f = cR_{\text{AHE}} + s^2 R_{\text{PHE}}\sin(2\phi_{\text{eq}}) \qquad (3)$$
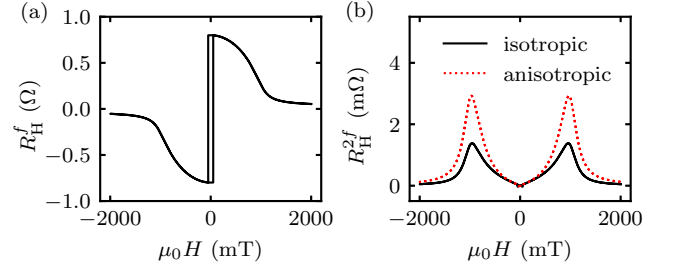

FIG. 2: Expected (a) first harmonic signal R_{H}^f and (b) second harmonic signal R_{H}^{2f}, the latter with and without higher order coefficients at $\phi_{\text{eq}} = 90°$, $\theta_b = 88°$. For the simulated SOT parameters see Tabs. I and II.

and

$$R_{\text{H}}^{2f} = (R_{\text{AHE}} - 2cR_{\text{PHE}}\sin(2\phi_{\text{eq}})) \\ \times \frac{\text{d}c}{\text{d}B_{\text{ext}}}\frac{1}{\sin(\theta_b - \theta_{\text{eq}})}B_\theta \qquad (4) \\ + s^2 R_{\text{PHE}}\frac{2\cos(2\phi_{\text{eq}})}{B_{\text{ext}}\sin(\theta_b)}B_\phi,$$

where we have assumed that the spin-torque-induced rotation angles are small. The parameters R_{AHE} and R_{PHE} are the coefficients for the anomalous and planar Hall resistance. Following Ref. 13, we use $R_{\text{AHE}} = 0.8\,\Omega$ and $R_{\text{PHE}} = 0.09\,\Omega$ in the simulations, representing a typical Pt/Co Hall bar structure. Moreover, B_θ and B_ϕ are the current-induced effective fields in the polar and azimuthal direction, respectively ($\mathbf{B}_I = B_\theta\hat{\mathbf{e}}_\theta + B_\phi\hat{\mathbf{e}}_\phi$), and are assumed to be proportional to the current amplitude I. Note that in real devices, thermal contributions to R_{H}^f and R_{H}^{2f} are often present. These contributions can be measured and subtracted before applying the analysis discussed below.[13,14]

To simulate harmonic measurement signals, we consider the limit of small excitations, where harmonics beyond the second order are negligible. In this scenario, we can eliminate the time-dependence from the simulation and instead calculate the expected signal from the static Hall resistance at constant current I via[13]

$$R_{\text{H}}^f = \frac{R_{\text{H}}(+I) + R_{\text{H}}(-I)}{2} \qquad (5)$$

and

$$R_{\text{H}}^{2f} = \frac{R_{\text{H}}(+I) - R_{\text{H}}(-I)}{2}. \qquad (6)$$

To calculate the static Hall resistance we numerically find a solution for $\mathbf{M}$ that minimizes the total effective field $\mathbf{B}_{\text{eff}}$ for a DC current. Examples of a simulated first and second harmonic signal are displayed in Fig. 2. The parameters used for the simulations are listed in Tabs. I and II. The perpendicular magnetic anisotropy

(PMA) field is fixed to $B_{\mathrm{K}} = 950\,\mathrm{mT}$ throughout this paper. The analysis uses the first harmonic Hall signals R_{H}^{f} at $\phi_{\mathrm{eq}} = 0°$, $45°$, $90°$ and the second harmonic signals R_{H}^{2f} at $\phi_{\mathrm{eq}} = 0°$, $90°$. The field is applied almost in-plane ($\theta_b = 88°$). The small out-of-plane contribution of the field prevents the formation of multi-domain states during measurements and stabilizes the numerical convergence of the simulations.

We first explain the established approach of extracting the parameters of Eqs. (1) and (2) from harmonic measurement data and illustrate the challenge of fitting anisotropic signals. We start by analytically inverting the symmetric and antisymmetric parts of Eq. (3) to extract the material parameters R_{AHE} and R_{PHE}, the cosine of the angle of magnetization $c = c(B_{\mathrm{ext}})$, and its derivative $\mathrm{d}c/\mathrm{d}B_{\mathrm{ext}}$ from $R_{\mathrm{H}}^{f,45}$, where the superscript denotes the polar field angle $\phi_{\mathrm{eq}} = 45°$.

Next, we analyze the second harmonic signal to extract $B_{0,2,4}^{\mathrm{FL}}$ and $B_{0,2,4}^{\mathrm{AD}}$. Unfortunately, there is no analytical means to this end, but this can be remedied as follows. Consider the simplest form of Eq. (4), which is obtained at $\phi_{\mathrm{eq}} = 0°$ and $90°$. At these angles, each single measurement of R_{H}^{2f} is related to two unknowns, B_θ and B_ϕ. We want to extract these from equation 4, but this is only possible by using the additional constraints of Eqs. (1) and (2), which tell us that B_θ and B_ϕ are related as follows:

$$B_\theta^{90} = c[B_0^{\mathrm{FL}} + s^2 B_2^{\mathrm{FL}} + s^4 B_4^{\mathrm{FL}}], \qquad (7)$$

$$B_\theta^0 = -[B_0^{\mathrm{AD}} + s^2 B_2^{\mathrm{AD}} + s^4 B_4^{\mathrm{AD}}], \qquad (8)$$

$$B_\phi^{90} = cB_0^{\mathrm{AD}}, \qquad (9)$$

$$B_\phi^0 = B_0^{\mathrm{FL}}, \qquad (10)$$

where again the superscripts 0 and 90 indicate the angle ϕ_{eq} in degrees. By measuring $R_{\mathrm{H}}^{2f}(\theta_{\mathrm{eq}}, \phi_{\mathrm{eq}})$ at $\phi_{\mathrm{eq}} = 0°$ and $90°$ and a sufficiently extensive set of angles θ_{eq}, the number of equations can exceed the number of unknowns. The established approach to solve these equations for $B_{0,2,4}^{\mathrm{FL}}$ and $B_{0,2,4}^{\mathrm{AD}}$ is an iterative procedure as illustrated in the flowchart of Fig. 3. This method, originally developed by Garello et al.[13], starts with with an initial guess (i) as follows:

i. Initially, all higher order contributions are ignored, i.e. $B_{2,4}^{\mathrm{FL,AD}} = 0$. Moreover, the process starts with a guess for B_ϕ^{90} to allow analytical inversion of Eq. (4). Since generally $R_{\mathrm{AHE}} \gg R_{\mathrm{PHE}}$, the contribution of the B_ϕ^{90} term to Eq. (4) is relatively small and we start with the initial guess $B_\phi^{90} = 0$ (we find that within reasonable bounds, this initial value of B_ϕ^{90} does not change the result of the analysis below).

Subsequently, the following steps are iterated:

1. B_θ^{90} is calculated by inverting equation (4) as

$$
\begin{aligned}
B_\theta^{90} = {} & \frac{\sin(\theta_b - \theta_{\mathrm{eq}})}{R_{\mathrm{AHE}}} \left(\frac{\mathrm{d}c}{\mathrm{d}B_{\mathrm{ext}}} \right)^{-1} \\
& \times \left[R_{\mathrm{H}}^{2f,90} + s^2 \frac{2R_{\mathrm{PHE}}}{B_{\mathrm{ext}} \sin(\theta_b)} B_\phi^{90} \right].
\end{aligned} \qquad (11)
$$

2. Using Eqs. (7) and (10) and the initial assumption of $B_{2,4}^{\mathrm{FL,AD}} = 0$, this result of B_θ^{90} is related to B_ϕ^0 via

$$B_\phi^0 = B_\theta^{90}/c. \qquad (12)$$

3. This now allows the use of the full Eq. (4) to calculate B_θ^0.

4. Then, using Eqs. (8) and (9) and $B_{2,4}^{\mathrm{FL,AD}} = 0$,

$$B_\phi^{90} = -cB_\theta^0. \qquad (13)$$

Steps 1 - 4 are repeated until the effective fields B_θ and B_ϕ for both angles converge. These iterations are performed independently for each value of the magnetization's azimuthal angle θ_{eq}. A final step yields the desired result:

5. The converged $B_\theta^{90}(\theta_{\mathrm{eq}})$ and $B_\theta^0(\theta_{\mathrm{eq}})$ are fitted to Eqs. (7) and (8) to extract $B_{0,2,4}^{\mathrm{FL}}$ and $B_{0,2,4}^{\mathrm{AD}}$, respectively.

We first test this method using the simulated harmonic measurements of an isotropic SOT system. The simulation parameters are listed in Tab. I. As expected, we find that the extracted values of $B_\theta^{0,90}(\theta_{\mathrm{eq}})$ are constant as a function of magnetization angle θ_{eq}, with a residual variation below 1% across the simulated field range. The fit to this data (step 5) accurately reproduces the simulation input values with relative errors Δ of approximately 0.02 %, see Tab. I.

However, the situation is very different when we assume significant contributions from anisotropic SOTs, see Tab. II for the simulation parameters. In this case, the extracted $B_\theta^{0,90}(\theta_{\mathrm{eq}})$ show a strong variation with the external field (Figs. 5b and d) and the resulting fit produces inaccurate results for the higher order SOT parameters (Tab. II). Note that the fit itself (step 5) is very accurate and falsely suggests that the resulting fit parameters are reliable (see fit errors listed in Tab. II). Contrary to this expectation, we find that in our example the extracted higher order coefficients deviate by up to 68 % from the input values of the simulation. This points to a convergence problem of the iterative calculation of the effective fields $B_\theta^{0,90}(\theta_{\mathrm{eq}})$ (steps 1-4) and, moreover, shows that the quality of the fit should
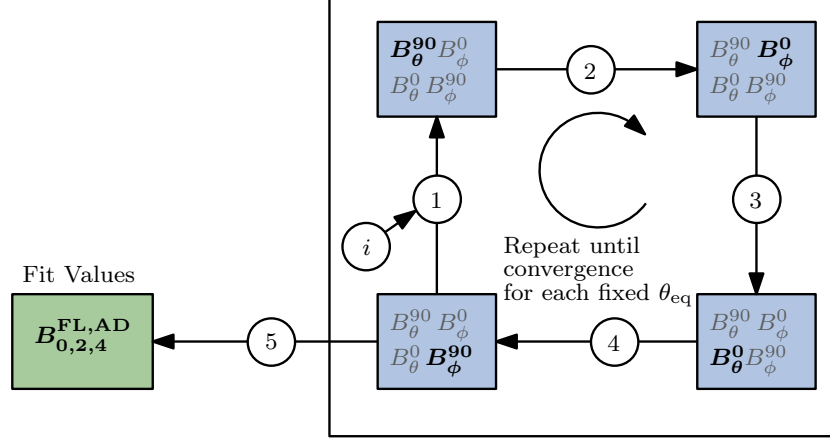
FIG. 3: Flowchart of the conventional iterative procedure to extract spin-orbit torques from harmonic measurements. The steps, indicated by the encircled numbers, are explained in the text. The updated quantities are printed in bold. Note that the fit of the desired torque coefficients is performed only once, after the boxed loop has reached convergence.

not be used to evaluate the error of the extracted SOT parameters. Next, we will develop a modified iterative process that accurately and reliably extracts higher order SOT coefficients.

The fundamental issue of the established analysis scheme of harmonic measurements is that anisotropic terms, if present, are not considered when calculating $B_\theta^{0,90}$ in the iterations. Here, we expand the process by a second layer of iterations in which the SOT coefficients $B_{0,2,4}^{AD}$ and $B_{0,2,4}^{FL}$ are allowed to change. This process is illustrated in Fig. 4. The starting point of this nested iterative process is the result generated by the conventional analysis, i.e. after converging to a stable solution.

Based on potentially non-zero higher order parameters $B_{2,4}^{FL,AD}$ extracted from the fit, we obtain new equations for the evaluation of steps 2 and 4:

2.*

$$B_\phi^0 = \frac{B_\theta^{90}}{c} - s^2 B_2^{FL} - s^4 B_4^{FL}, \qquad (14)$$

4.*

$$B_\phi^{90} = -c\big(B_\theta^0 + s^2 B_2^{AD} + s^4 B_4^{AD}\big). \qquad (15)$$

These equations refine the conventional (inner) loop of the iterative analysis scheme (Fig. 4). For each set of higher order parameters $B_{2,4}^{FL,AD}$, this inner loop is repeated until convergence of B_θ and B_ϕ is obtained. Only then are $B_{0,2,4}^{FL,AD}$ updated by executing step 5. With each updated set of parameters $B_{2,4}^{FL,AD}$, the inner loop is started again. The final result is the set of all $B_{0,2,4}^{FL,AD}$ coefficients obtained after convergence of the outer loop.

We find that this separation of an inner loop with constant $B_{2,4}^{FL,AD}$ is key for the robust convergence of the entire analysis.

TABLE I: Simulation and analysis of a purely isotropic SOT system. The table lists the input SOT parameters (in mT) as well as the values extracted from the conventional and nested iterative analysis of the simulated harmonic signals. We also show the fit residual standard error (σ, in mT) and the deviation between analysis result and the input value normalized to the input value (Δ, in per cent) for both analysis methods.

		Conventional			Nested		
Input		Result	σ	Δ (%)	Result	σ	Δ (%)
B_0^{FL}	-1.2	-1.20	1×10^{-6}	-0.02	-1.20	1×10^{-6}	-0.02
B_2^{FL}	0	0.00	1×10^{-5}	-	0.00	1×10^{-5}	-
B_4^{FL}	0	0.00	1×10^{-5}	-	0.00	1×10^{-5}	-
B_0^{AD}	1.9	1.90	2×10^{-6}	0.02	1.90	2×10^{-6}	0.02
B_2^{AD}	0	0.00	1×10^{-5}	-	0.00	1×10^{-5}	-
B_4^{AD}	0	0.00	1×10^{-5}	-	0.00	1×10^{-5}	-

The nested iterative analysis does not significantly influence the extracted values for purely isotropic SOTs (Tab. I and Fig. 5a and c). However, if anisotropic SOT components are present, every time we restart a new iteration, the newly fitted coefficients improve the accuracy of the conversion rules in Eqs. (14) and (15). Consequently, we are now able to converge precisely to the simulated expressions as shown in Tab. II and illustrated in Figs. 5b and d. The relative deviation of the determined coefficients from the simulated input is
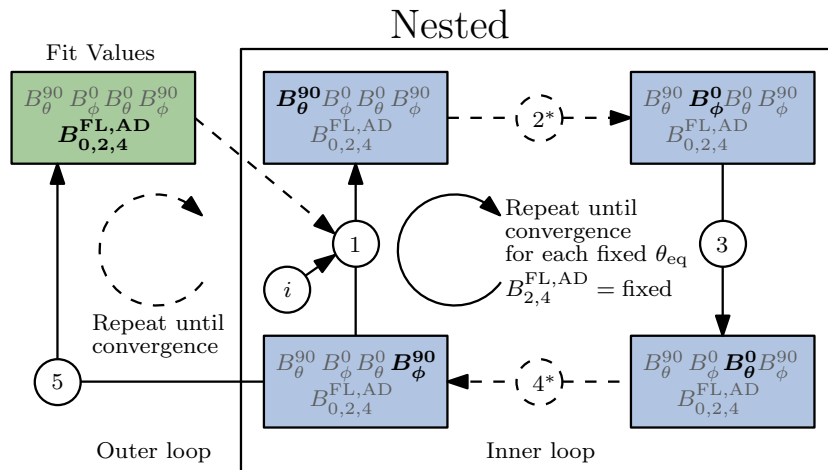
FIG. 4: Flowchart of the nested iterative procedure to extract spin-orbit torques from harmonic measurements. Updated steps in the nested iterative procedure are highlighted as dashed lines (as compared to the conventional procedure). The steps, indicated by the encircled numbers, are explained in the text. The updated quantities are in bold. Note that for each iteration of the outer loop, the conventional procedure in the inner loop converges.

TABLE II: Simulation and analysis of an anisotropic SOT system. The table lists the input SOT parameters (in mT) as well as the values extracted from the conventional and nested iterative analysis of the simulated harmonic signals. We also show the fit residual standard error (σ, in mT) and the deviation between analysis result and simulated SOT value normalized to the input value (Δ, in per cent) for both analysis methods.

		Conventional			Nested		
Input		Result	σ	Δ (%)	Result	σ	Δ (%)
B_0^{FL}	-1.2	-1.20	5×10^{-6}	0.08	-1.20	1×10^{-6}	-0.01
B_2^{FL}	-1.1	-1.41	4×10^{-5}	-28	-1.10	1×10^{-5}	0.04
B_4^{FL}	-0.4	-0.13	6×10^{-5}	68	-0.40	1×10^{-5}	-0.08
B_0^{AD}	1.9	1.90	3×10^{-6}	-0.01	1.90	3×10^{-6}	0.006
B_2^{AD}	1.0	1.32	2×10^{-5}	32	1.00	2×10^{-5}	0.07
B_4^{AD}	0.6	0.30	4×10^{-5}	-50	0.60	3×10^{-5}	-0.8

FIG. 5: SOT fields extracted from the conventional and nested iterative analysis as a function of magnetization angle $\sin^2 \theta_{\mathrm{eq}}$. Figures (a) and (c) show the results for the isotropic SOTs (see parameters in Tab. I). Figures (b) and (d) show the fields extracted from the anisotropic SOT simulation (see Tab. II). The functional dependence expected from the known input parameters is plotted with solid lines. The extracted torque coefficients are listed in the Tabs I and II.

now below 1% across all orders of the SOT parameters used here. The nested iterative procedure not only yields more accurate results than the conventional analysis, it also runs fully automatically and with little computational cost on any personal computer. It is therefore highly recommended to always use the nested iterative procedure when extracting SOTs from harmonic measurements.

Lastly, we investigate the influence of noise, as always present in experimental data, on the precision of the nested analysis. To this end, we added sets of random, normall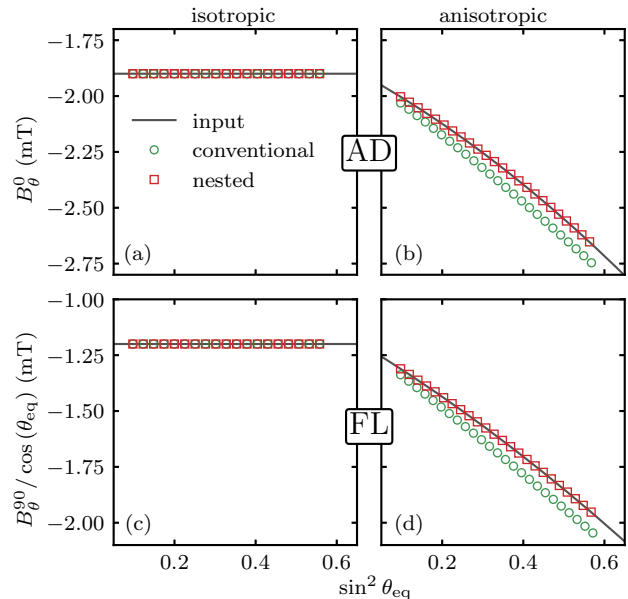y distributed noise (with a mean value of zero and standard deviation σ_{noise}) to the simulated first and second harmonic signals. For every value of σ_{noise} twenty different sets of noisy measurement data were generated and from each data set we extracted
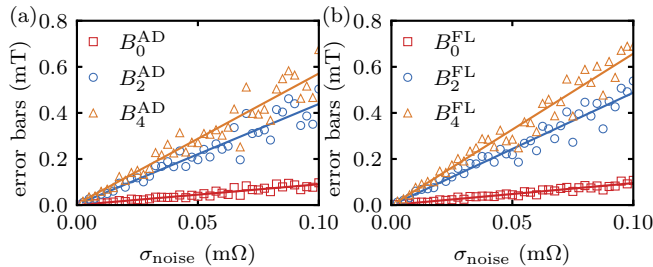
FIG. 6: Error bars of the extracted SOT parameters in the presence of experimental noise σ_{noise}. The simulation input parameters are listed in Tab. II and σ_{noise} was added to the simulated first and second harmonic signals (see Fig. 2, sampled in 1 mT steps). Panels (a) and (b) show the results and linear fits for $B_{0,2,4}^{\text{AD}}$ and $B_{0,2,4}^{\text{FL}}$, respectively.

the SOT parameters using our nested iterative analysis scheme. Subsequently, we calculated the error bars of each SOT parameter x (with $x = B_{0,2,4}^{\text{FL,AD}}$) via $\sigma_x = \sqrt{1/(n-1)\sum_{i=1}^{n}(x - x_{\text{input}})^2}$, where x_{input} is the noise-free input parameter and $n = 20$ in our example. That is, σ_x is the standard deviation of x with respect to x_{input}. As shown in Fig. 6, we find a linear dependence on σ_{noise}. Importantly, for $\sigma_{\text{noise}} \leq 0.01\,\text{m}\Omega$, as realistically achievable in carefully measured Hall signals[13], the uncertainty is sufficiently low (error bars $\leq 0.07\,\text{mT}$) to retrieve a good estimate for all SOT parameters considered here.

To conclude, we have shown by means of simulations that the values of higher order spin-orbit torque coefficients extracted via the established iterative procedure from harmonic measurements may not be reliable. To overcome these issues, we have proposed a modified analysis scheme that allows the anisotropic terms to vary during the iterations and to converge to their correct values. We found that a nested iterative implementation of the algorithm is required to make this convergence robust. We have verified our approach by means of simulations, which show that our procedure yields accurate, self-consistent results even in the presence of sizable higher order terms. A fully automated code to use this analysis is openly available.[26] Our method enables high-precision measurements of anisotropic SOTs, thus paving the way for a deeper understanding of the fundamental physics underlying these torques and for their application in tailored spintronics devices.

The data that support the findings of this study are openly available in Zenodo at http://doi.org/10.5281/zenodo.4648462.

[1] J. Sinova and I. Žutić, "New moves of the spintronics tango," Nature Materials **11**, 368–371 (2012).

[2] A. Manchon, J. Železný, I. M. Miron, T. Jungwirth, J. Sinova, A. Thiaville, K. Garello, and P. Gambardella, "Current-induced spin-orbit torques in ferromagnetic and antiferromagnetic systems," Reviews of Modern Physics **91**, 035004 (2019).

[3] L. Liu, C. F. Pai, Y. Li, H. W. Tseng, D. C. Ralph, and R. A. Buhrman, "Spin-torque switching with the giant spin hall effect of tantalum," Science **336**, 555–558 (2012).

[4] I. M. Miron, K. Garello, G. Gaudin, P. J. Zermatten, M. V. Costache, S. Auffret, S. Bandiera, B. Rodmacq, A. Schuhl, and P. Gambardella, "Perpendicular switching of a single ferromagnetic layer induced by in-plane current injection," Nature **476**, 189–193 (2011).

[5] F. Büttner, I. Lemesh, M. Schneider, B. Pfau, C. M. Günther, P. Hessing, J. Geilhufe, L. Caretta, D. Engel, B. Krüger, J. Viefhaus, S. Eisebitt, and G. S. D. Beach, "Field-free deterministic ultrafast creation of magnetic skyrmions by spin-orbit torques," Nature Nanotechnology **12**, 1040–1044 (2017).

[6] S. Woo, K. M. Song, X. Zhang, M. Ezawa, Y. Zhou, X. Liu, M. Weigand, S. Finizio, J. Raabe, M. C. Park, K. Y. Lee, J. W. Choi, B. C. Min, H. C. Koo, and J. Chang, "Deterministic creation and deletion of a single magnetic skyrmion observed by direct time-resolved X-ray microscopy," Nature Electronics **1**, 288–296 (2018).

[7] K. S. Ryu, L. Thomas, S. H. Yang, and S. Parkin, "Chiral spin torque at magnetic domain walls," Nature Nanotechnology **8**, 527–533 (2013).

[8] S. Emori, U. Bauer, S. M. Ahn, E. Martinez, and G. S. D. Beach, "Current-driven dynamics of chiral ferromagnetic domain walls," Nature Materials **12**, 611–616 (2013).

[9] K. Litzius, I. Lemesh, B. Krüger, P. Bassirian, L. Caretta, K. Richter, F. Büttner, K. Sato, O. A. Tretiakov, J. Förster, R. M. Reeve, M. Weigand, I. Bykova, H. Stoll, G. Schütz, G. S. D. Beach, and M. Kläui, "Skyrmion Hall effect revealed by direct time-resolved X-ray microscopy," Nature Physics **13**, 170–175 (2017).

[10] S. Woo, K. M. Song, H. S. Han, M. S. Jung, M. Y. Im, K. S. Lee, K. S. Song, P. Fischer, J. I. Hong, J. W. Choi, B. C. Min, H. C. Koo, and J. Chang, "Spin-orbit torque-driven skyrmion dynamics revealed by time-resolved X-ray microscopy," Nature Communications **8**, 1–8 (2017).

[11] W. Legrand, D. Maccariello, N. Reyren, K. Garcia, C. Moutafis, C. Moreau-Luchaire, S. Collin, K. Bouzehouane, V. Cros, and A. Fert, "Room-Temperature Current-Induced Generation and Motion of sub-100 nm Skyrmions," Nano Letters **17**, 2703–2712 (2017).

[12] W. Jiang, X. Zhang, G. Yu, W. Zhang, X. Wang, M. Benjamin Jungfleisch, J. E. Pearson, X. Cheng, O. Heinonen, K. L. Wang, Y. Zhou, A. Hoffmann, and S. G. E. Te Velthuis, "Direct observation of the skyrmion Hall effect," Nature Physics **13**, 162–169 (2017).

[13] K. Garello, I. M. Miron, C. O. Avci, F. Freimuth, Y. Mokrousov, S. Blügel, S. Auffret, O. Boulle, G. Gaudin, and P. Gambardella, "Symmetry and magnitude of spin-orbit torques in ferromagnetic heterostructures," Nature Nanotechnology **8**, 587–593 (2013).

[14] C. O. Avci, K. Garello, M. Gabureac, A. Ghosh, A. Fuhrer, S. F. Alvarado, and P. Gambardella, "Interplay of spin-orbit torque and thermoelectric effects in ferromagnet/normal-metal bilayers," Physical Review B **90**, 224427 (2014).

[15] X. Qiu, P. Deorani, K. Narayanapillai, K. S. Lee, K. J. Lee, H. W. Lee, and H. Yang, "Angular and temperature dependence of current induced spin-orbit effective fields in Ta/CoFeB/MgO nanowires," Scientific Reports **4**, 4491 (2014).

[16] S. Ghosh and A. Manchon, "Spin-orbit torque in a three-dimensional topological insulator-ferromagnet heterostructure: Crossover between bulk and surface transport," Physical Review B **97**, 134402 (2018).

[17] H. K. Gweon, K. J. Lee, and S. H. Lim, "Influence of Mg O Sputtering Power and Post annealing on Strength and Angular Dependence of Spin-Orbit Torques in Pt/Co/Mg O Trilayers," Physical Review Applied **11**, 014034 (2019).

[18] T. Schulz, K. Lee, B. Krüger, R. Lo Conte, G. V. Karnad, K. Garcia, L. Vila, B. Ocker, D. Ravelosona, and M. Kläui, "Effective field analysis using the full angular spin-orbit torque magnetometry dependence," Physical Review B **95**, 224409 (2017).

[19] C. Ortiz Pauyac, X. Wang, M. Chshiev, and A. Manchon, "Angular dependence and symmetry of Rashba spin torque in ferromagnetic heterostructures," Applied Physics Letters **102**, 252403 (2013).

[20] P. M. Haney, R. A. Duine, A. S. Núñez, and A. H. MacDonald, "Current-induced torques in magnetic metals: Beyond spin-transfer," Journal of Magnetism and Magnetic Materials **320**, 1300–1311 (2008).

[21] V. P. Amin and M. D. Stiles, "Spin transport at interfaces with spin-orbit coupling: Formalism and Phenomenology," Physical Review B **94**, 104419 (2016).

[22] J. P. Hanke, F. Freimuth, B. Dupé, J. Sinova, M. Kläui, and Y. Mokrousov, "Engineering the dynamics of topological spin textures by anisotropic spin-orbit torques," Physical Review B **101**, 1–8 (2020).

[23] E. S. Park, D. K. Lee, B. C. Min, and K. J. Lee, "Elimination of thermoelectric artifacts in the harmonic Hall measurement of spin-orbit torque," Physical Review B **100**, 214438 (2019).

[24] M. Hayashi, J. Kim, M. Yamanouchi, and H. Ohno, "Quantitative characterization of the spin-orbit torque using harmonic Hall voltage measurements," Physical Review B **89**, 144425 (2014).

[25] C. O. Avci, K. Garello, C. Nistor, S. Godey, B. Ballesteros, A. Mugarza, A. Barla, M. Valvidares, E. Pellegrin, A. Ghosh, I. M. Miron, O. Boulle, S. Auffret, G. Gaudin, and P. Gambardella, "Fieldlike and antidamping spin-orbit torques in as-grown and annealed Ta/CoFeB/MgO layers," Physical Review B - Condensed Matter and Materials Physics **89**, 1–13 (2014).

[26] D. M. J. van Elst, M. R. A. Peters, F. Büttner, A. Wittman, E. A. Tremsina, C. Avci, R. Lavrijsen, H. J. M. Swagten, and G. S. D. Beach, "Accurate Extraction of Anisotropic Spin-Orbit Torques from Harmonic Measurements," Zenodo (2021), http://doi.org/10.5281/zenodo.4648462.